Nonlinear Planetary Wave Reflection in an Atmospheric GCM

CHRISTOPHER C. WALKER AND GUDRUN MAGNUSDOTTIR

Department of Earth System Science, University of California, Irvine, Irvine, California

(Manuscript received 17 April 2002, in final form 16 July 2002)

ABSTRACT

The nonlinear behavior of planetary waves excited by midlatitude topography is considered in an atmospheric GCM. The GCM is run at standard resolution (T42) and includes all of the complexity normally associated with a GCM. Only two simplifications are made to the model. First, it is run in perpetual January mode, so that the solar radiation takes the diurnally varying value associated with 15 January. Second, the lower boundary is simplified so that it is entirely ocean with zonally symmetric SSTs. Planetary waves are excited by Gaussian-shaped topography centered at 45°N, 90°W. As in earlier studies, the excited wave train propagates toward low latitudes where, for sufficiently large forcing amplitude (i.e., height of topography), the wave will break. Several different experiments are run with different mountain heights. Each experiment is run for a total of 4015 days.

The response of the model depends on the height of the mountain. For the small-amplitude mountain (500 m), the wave is dissipated at low latitudes near its critical latitude. For large-amplitude mountains (2000, 3000, and 4000 m), wave breaking and nonlinear reflection out of the wave breaking region is observed. The spatial character of the reflected wave train is similar to that detected in earlier studies with more idealized models.

1. Introduction

This paper investigates whether nonlinear planetary wave reflection plays a role in establishing longitudinal asymmetries in the time-mean circulation of the wintertime extratropical troposphere. It has long been known that longitudinal asymmetries are produced by planetary waves excited by the earth's topography and by quasi-stationary longitudinal variations in heating (Charney and Eliassen 1949; Smagorinsky 1953). As shown in Charney and Eliassen (1949) and in a number of more recent studies (e.g., Held 1983), linear planetary wave theory appears to work well in explaining longitudinal asymmetries. Linear theory holds that planetary waves are excited in midlatitudes and propagate to low latitudes, where they are absorbed near their critical latitude, the latitude at which the background zonal wind matches the zonal phase speed of the wave (e.g., Killworth and McIntyre 1985). However, observations have shown that intense nonlinear wave breaking can take place in low latitudes (e.g., Postel and Hitchman 1999; Waugh and Polvani 2000).

It is not clear how these nonlinear wave breaking regions modify the linear description of the wintertime circulation. There is growing evidence that wave breaking at low latitudes may lead to nonlinear reflection, such that reflected waves propagate out of the wave breaking region into midlatitudes. Brunet and Haynes (1996) found nonlinear reflection of an isolated wave train in a shallow water model. They considered the simple case of zonally symmetric initial flow representing the wintertime upper troposphere. This study was extended to three dimensions by Magnusdottir and Haynes (1999), who used a primitive equation model to investigate wave reflection in baroclinic flows. Magnusdottir and Haynes (1999) found evidence for nonlinear reflection in realistic baroclinic flows.

Magnusdottir and Haynes (1999) and Brunet and Haynes (1996) both investigated reflection without a representation of the Hadley circulation. Both studies suggest that nonconservative aspects of the Hadley circulation would dissipate wave activity and therefore act against wave reflection. Subsequent studies by Esler et al. (2000) and Magnusdottir and Walker (2000) in a shallow water model, and Walker and Magnusdottir (2002) in a primitive equation model investigated the effect of the Hadley circulation on nonlinear wave reflection. These studies conclude that the Hadley circulation damps wave reflection, but that given sufficient forcing, nonlinear wave reflection will still occur.

All of the modeling studies discussed thus far are initial value problems with zonally symmetric initial states. In the three-dimensional studies (Magnusdottir and Haynes 1999; Walker and Magnusdottir 2002), the growth of transient baroclinic disturbances was inhibited by applying Rayleigh friction on the lowest model levels. Thus the role of baroclinic disturbances was not considered even though they have been found to provide

Corresponding author address: Dr. Gudrun Magnusdottir, Department of Earth System Science, University of California, Irvine, Irvine, CA 92697-3100.
E-mail: gudrun@uci.edu

important feedback on low-frequency variability (e.g., Branstator 1992).

There have been some attempts to identify nonlinear reflection in general circulation model (GCM) experiments where high-frequency transients are not suppressed. Schneider (1990) analyzed GCM simulations by using a linear stationary wave model based on the GCM. Using comparisons of the full GCM results with results from the linearized model, he concluded that nonlinear reflection from a low-latitude critical line was possible. Cook and Held (1992, hereafter CH92) used a low-resolution (R15) aquaplanet GCM, forced with annual-mean solar radiation, to investigate the role of nonlinearities on orographically forced planetary waves. CH92 did not find any evidence of reflection, but suggested that the background flow and the coarse resolution of the model may have underestimated the potential for nonlinear reflection.

Here we examine nonlinear wave reflection in an atmospheric GCM, building on our earlier more idealized studies. We use a high-resolution GCM that has all of the complexity included in a state-of-the-art GCM. Our only simplifications are that we run the model in perpetual January mode and we consider an idealized lower boundary. A wave train is excited in midlatitudes by a single Gaussian mountain. We use several different mountain heights and observe the response of the model as the height of the mountain is increased. Consistent with earlier studies in more idealized models, we find strong evidence of nonlinear reflection for large-amplitude forcing.

The plan of this paper is as follows. In section 2, we discuss the model configuration, parameter settings, and experimental setup. In section 3 we present our numerical results. Section 4 summarizes our findings and comments on the potential for nonlinear reflection in the real atmosphere. The experiments reported here are similar to those in CH92, but with different conclusions. Section 4 therefore contains a comparison of CH92 and our results.

2. Model and parameters

We use version 3.10.11 of the National Center for Atmospheric Research's (NCAR) Community Climate Model (CCM3), run at a horizontal resolution of T42, with 18 vertical levels. The model is run in a perpetual January aquaplanet configuration with zonally symmetric sea surface temperatures (SSTs). [A similar model configuration is discussed in Yin and Battisti (2001).] The zonally symmetric SSTs are generated by averaging, for a given northern latitude, the observed January SSTs with the observed July SSTs at the same latitude in the Southern Hemisphere. [The observed SSTs are documented in Shea et al. (1990).] For example, the SST for all longitudes at 30°N is the average of the 30°N January values and the 30°S July values. Likewise, the SST for all longitudes at 30°S is the average of the 30°S January values and the 30°N July values. Sea ice is prescribed in the model when the SST drops below −1.8°C. If sea ice is present at more than half of the grid points at both latitudes, then the entire latitude circle is set to have sea ice. Note that although the model is forced with axisymmetric SSTs, atmospheric processes such as transient baroclinic disturbances and tropical convection introduce significant zonal asymmetry in the overlying atmosphere.

Topography is included in the model with a Gaussian ''ocean mountain'' that has a half-width of 1066 km located at 45°N, 90°W (identically shaped topography is considered in Walker and Magnusdottir 2002; Magnusdottir and Walker 2000; Magnusdottir and Haynes 1999; Brunet and Haynes 1996). To prevent warm SSTs from occurring at high elevations, we decrease the SST by 6.5 K km^{-1} in the vicinity of the topography. We consider several different maximum mountain heights, ranging from 0 to 5000 m, although here we concentrate on results for heights of 500, 2000, 3000, and 4000 m. For each mountain height, the model is run for a total of 4015 days, where each day has the diurnally varying solar radiation associated with 15 January. The model comes to a statistical steady state within 90 days, but the first 180 days are disregarded to ensure that the transient effects of spinning up the model are eliminated. This leaves a total of 3835 days for each case.

The coefficient of ∇^2 diffusion applied in the top three layers of the model is increased from the default value of 2.5×10^5 m^2 s^{-1} to 3.75×10^5 m^2 s^{-1} to mimic the effects of gravity wave drag. The ∇^2 diffusion is present only above 64 mb; therefore, it does not significantly affect the results presented here, which are concerned with nonlinear wave reflection in the troposphere. A ∇^4 hyperdiffusion with a coefficient of 10^{16} m^4 s^{-1} on the smallest horizontal scales is applied on all other model levels to prevent spectral blocking.

The model configuration discussed above yields zonal and meridional winds that are reasonably close to observed wintertime conditions. In the following, we indicate a time mean by an overbar and the deviation from the time mean by a prime, such that $x = \overline{x} + x'$ for any quantity x. We indicate a zonal average by square brackets and the deviation from the zonal average by a star, such that $x = [x] + x^\star$. Figure 1a shows $[\overline{u}]$ for the case without topography. As shown in Fig. 1a, the tropospheric jet is similar in magnitude and location to the observed wintertime jet. Furthermore, as in observations, easterlies are present at all levels in the Tropics, guaranteeing that an equatorward propagating quasi-stationary planetary wave train will encounter a critical line. Unlike the real atmosphere, tropical westerlies are not found at any longitudes in the time-mean flow field so that linear propagation across the equator is not possible.

Although there is qualitative agreement between the observed wintertime zonally averaged zonal wind and $[\overline{u}]$ shown in Fig. 1a, there are some quantitative dis-

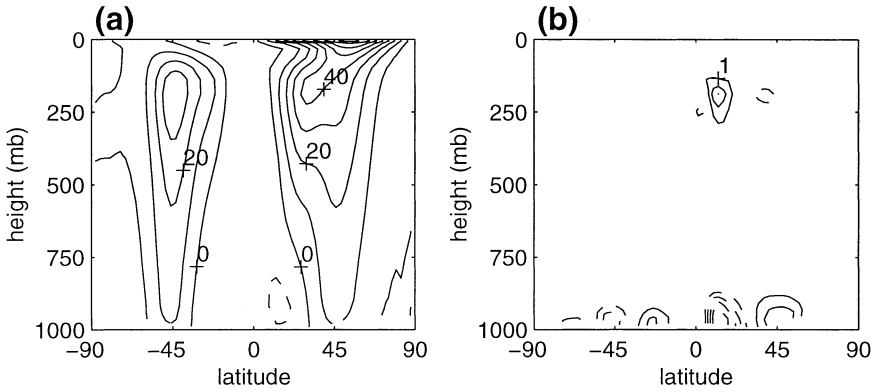

FIG. 1. Zonal and time (3835 days) average of (a) zonal and (b) meridional wind for case without topography. Contour interval is (a) 10 m s^{-1} and (b) 1.0 m s^{-1} (zero contour omitted). Dashed contours correspond to negative values.

crepancies. First, even with increased ∇^2 diffusion, $[\overline{u}]$ in the stratospheric jet is excessive, reaching a maximum value of 83 m s^{-1} on the uppermost model level. The strength of the stratospheric jet decreases markedly when topography is present, but even in the 4000-m case (not shown), the maximum value of $[\overline{u}]$ is still 58 m s^{-1}. As discussed in section 1, we are concerned with planetary wave reflection in the troposphere. At the tropopause level, $[\overline{u}]$ is in agreement with observations; it is only in the midstratosphere that it becomes unrealistic.

The surface $[\overline{u}]$ in the region of the topographical forcing (45°N) is too large, with a maximum value of approximately 15 m s^{-1}. This is a potentially more serious discrepancy than the excessive stratospheric wind speeds, since the amplitude of a topographically generated planetary wave depends on the wind in this region. However, even for our strongest forcing (5000 m), the wave amplitudes are consistent with observations.

Several recent studies have shown that the Hadley circulation inhibits nonlinear planetary wave reflection (Walker and Magnusdottir 2002; Magnusdottir and Walker 2000; Esler et al. 2000). A realistic Hadley circulation is therefore of primary importance to this study. As shown in Fig. 1b, the time mean of the zonally averaged meridional wind for the control case $[\overline{v}]$ shows a Hadley circulation that is consistent with observations, with a maximum northward windspeed of approximately 3 m s^{-1}. It is slightly narrower in latitudinal extent than the observed wintertime Hadley circulation. On the 200-mb surface, however, the zero-wind line is south of the maximum meridional wind, so an equatorward propagating stationary wave experiences significant opposing flow before reaching its critical line. We therefore believe that the damping associated with the Hadley circulation is well represented in these experiments.

3. Results

Figure 2a shows the time-averaged eddy meridional wind $\overline{v}^{\star}$ on the 200-mb surface for the case forced with the 500-m mountain. The response is broadly similar to earlier work on linear planetary wave propagation (e.g., Grose and Hoskins 1979), with a wave propagating from the topographical region eastward and toward the equator. This wave is absorbed near its critical line (approximately 10°N at 200 mb) with no sign of reflection. Unlike Grose and Hoskins (1979), Fig. 2a does not show a poleward propagating wave. CH92 also did not observe a poleward propagating wave train in their small-amplitude case.

The time-averaged potential vorticity (PV) field on the 345-K isentropic surface, shown in Fig. 2b, is consistent with indefinite low-latitude absorption. Nonlinear reflection is associated with overturning PV contours caused by breaking waves (e.g., Killworth and McIntyre 1985). In this case, the PV field where the waves impact the critical line (around 15°N, 150°E) is only slightly disturbed and does not show signs of wave breaking. Even though the meridional gradient of PV in this area is weak [note that the contour interval in Fig. 2b is 0.1 potential vorticity unit (PVU) near the critical line, and 0.5 PVU elsewhere], and therefore amenable to overturning, the amplitude of the incident wave train is not large enough to irreversibly mix PV.

As the height of the topography is increased, the response diverges from the small-amplitude response. The departure manifests itself in the 200-mb $\overline{v}^{\star}$ primarily in two ways. First, an additional wave train appears to the north of the topography. This is most visible in the 3000- and 4000-m cases (Figs. 3b and 3c, respectively), where a wave is seen propagating from the topography east and toward the pole. The appearance of a poleward-propagating wave was observed and explained by CH92.

The second departure from the small-amplitude response was not present in CH92. It is a wave train that propagates out of low latitudes toward midlatitudes. This wave train is easily seen in the 3000- and 4000-m cases, where a wave train originating around 30°N, 180°, propagates northeast into midlatitudes. We believe

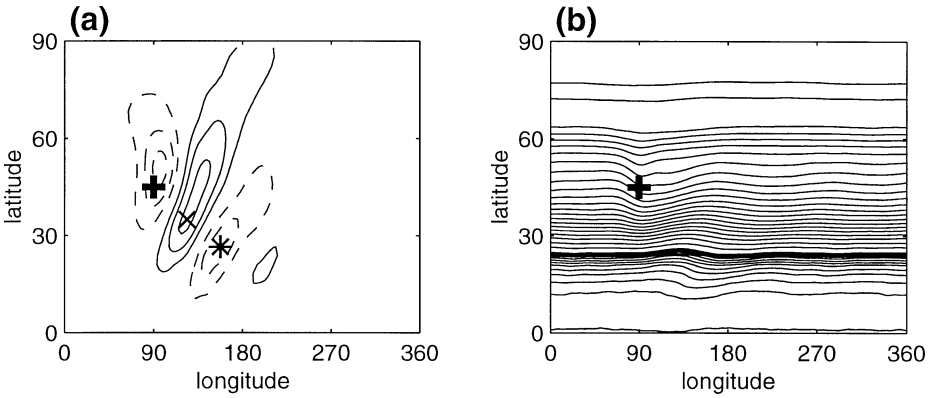

FIG. 2. Mountain height is 500 m. (a) Time-mean meridional wind with the zonal average removed ($\overline{v}^{\star}$) on 200-mb surface and (b) time-mean PV on 345K isentropic surface (corresponds roughly to the 200-mb surface south of 45°N) for 500-m topography. Contour interval in (a) is 1.0 m s^{-1}. Contour interval in (b) is 0.1 PVU (1 PVU = 10^{-6} m^2 s^{-1} K kg^{-1}) from 0 to 1 PVU (south of approximately 25°N), and 0.5 PVU above 1.0 PVU (1 PVU is shown with a thick solid contour). The center of the topography is indicated in both panels with a heavy + symbol. The × and * in (a) mark the basis points for the lag correlations shown in Figs. 5 and 6a, respectively.

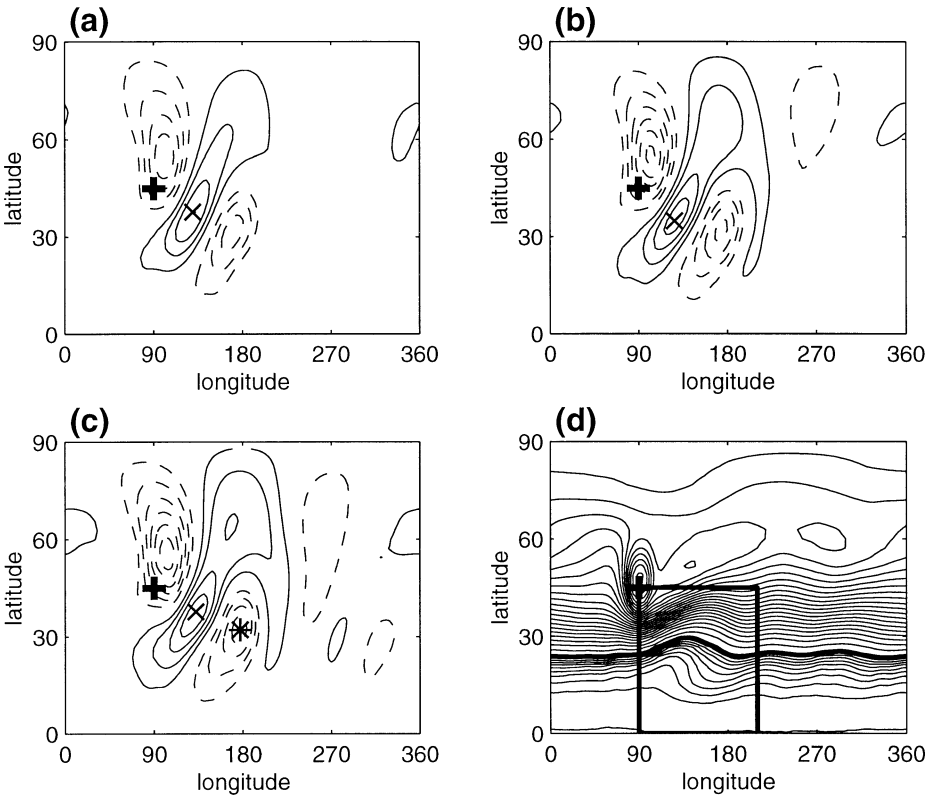

FIG. 3. ($\overline{v}^{\star}$) on 200-mb surface for (a) 2000-m topography, (b) 3000-m topography, and (c) 4000-m topography. (d) Time-averaged PV on 345-K isentropic surface for 4000-m case. Contour interval in (a)–(c) is 2.0 m s^{-1}. Contour interval in (d) is the same as Fig. 2b. The × in (a)–(c) indicates the basis point for lag correlations shown in Fig. 5. The * in (c) is the location of the basis point for the lag correlation shown in Fig. 6b. The box in (d) demarcates the region shown in Fig. 4.

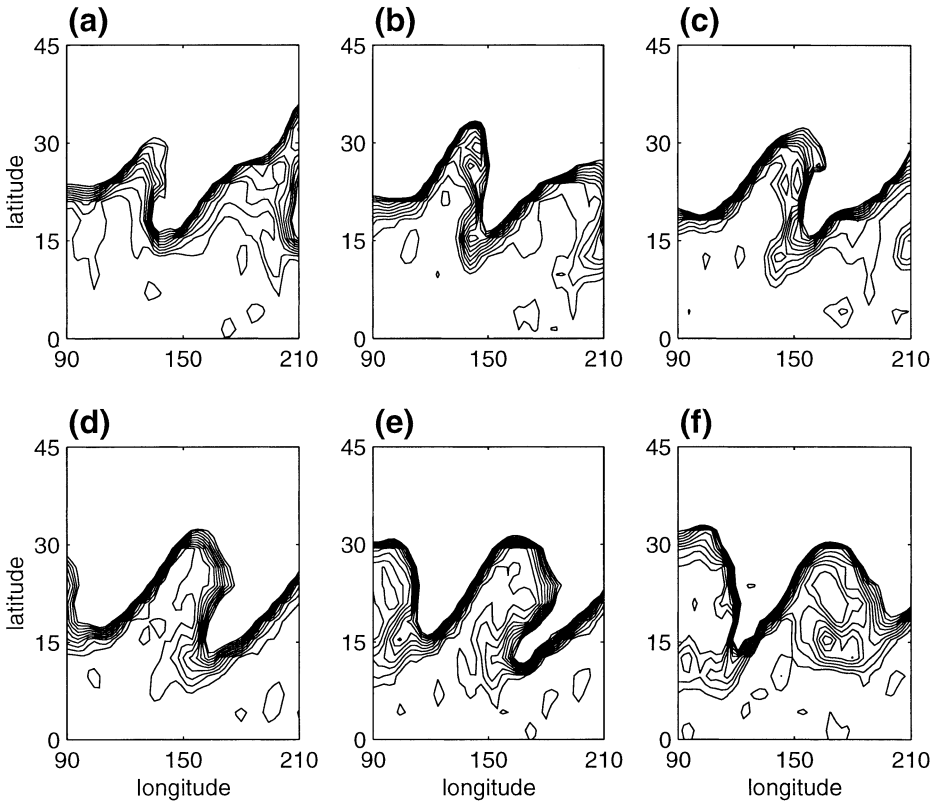

FIG. 4. Instantaneous view of PV on 345-K isentropic surface for 4000-m mountain. (a)–(f) Six consecutive days are shown, starting with (a). Only PV from 0.1 to 1.0 PVU is shown, with a contour interval of 0.1 PVU.

that this wave train is a result of the nonlinear reflection of the topographically forced planetary wave.

As mentioned earlier, nonlinear reflection is associated with overturning PV contours. In this regard, the PV field for the 4000-m mountain is consistent with reflection out of low latitudes. The time-averaged PV field for the 4000-m case, shown in Fig. 3d, is considerably more disturbed where the wave is incident on the critical layer (near 20°N, 150°E) than the corresponding PV field for the 500-m case (Fig. 2b). The mean low-latitude PV pattern seen in Fig. 3d is a product of repeated wave breaking. A typical breaking event is seen in Figs. 4a–f, which show the instantaneous PV field on six consecutive days. Early in this sequence (Figs. 4a and 4b), the PV field does not yet show signs of irreversible mixing. Indeed, there are other instances (not shown) where the PV evolved to a state similar to that shown in Figs. 4a and 4b and then reverted to a more zonal configuration. As the sequence continues, however, it becomes clear that PV is being irreversibly rearranged and the PV field can no longer support linear wave propagation. The wave eventually breaks, such that on the final day of the sequence (Fig. 4f), the ribbon of steep PV gradients no longer shows the overturning, present in Figs. 4c–e, that characterizes wave breaking. In addition, the PV field shows very small spatial scales, with isolated patches of high PV air at low latitudes (around 15°N, 170°E), in the wave breaking region. It should be noted that the breaking event shown in Figs. 4a–f is a typical event in a quasi-periodic time sequence reminiscent of the limit cycle observed in Held and Phillips (1990).

Evidence of reflection out of the wave breaking region is corroborated with lagged correlations of the 200-mb eddy meridional wind. The use of lagged correlations to track wave propagation is familiar from earlier work by, for example, Blackmon et al. (1984) and Randel (1987). We choose as a basis point the location of maximum eddy meridional wind, which is marked on Figs. 2a and 3a–c with a $\times$ symbol. Lag correlations with this basis point are shown in Fig. 5 for the 500-, 2000-, 3000-, and 4000-m mountains. The long time series (3835 days) leads to high significance; all results shown are significant at the 95% confidence level.

First consider the lag correlations for the 500-m mountain (top row in Fig. 5). In this case, a wave propagates from the topography southeast though the basis point and is dissipated in low latitudes near its critical line. This is contrasted with the 3000- and 4000-m cases, where a wave is clearly seen propagating in an arc out of the wave breaking region (around 30°N, 150°E) toward the midlatitudes; turning southward near 45°N,

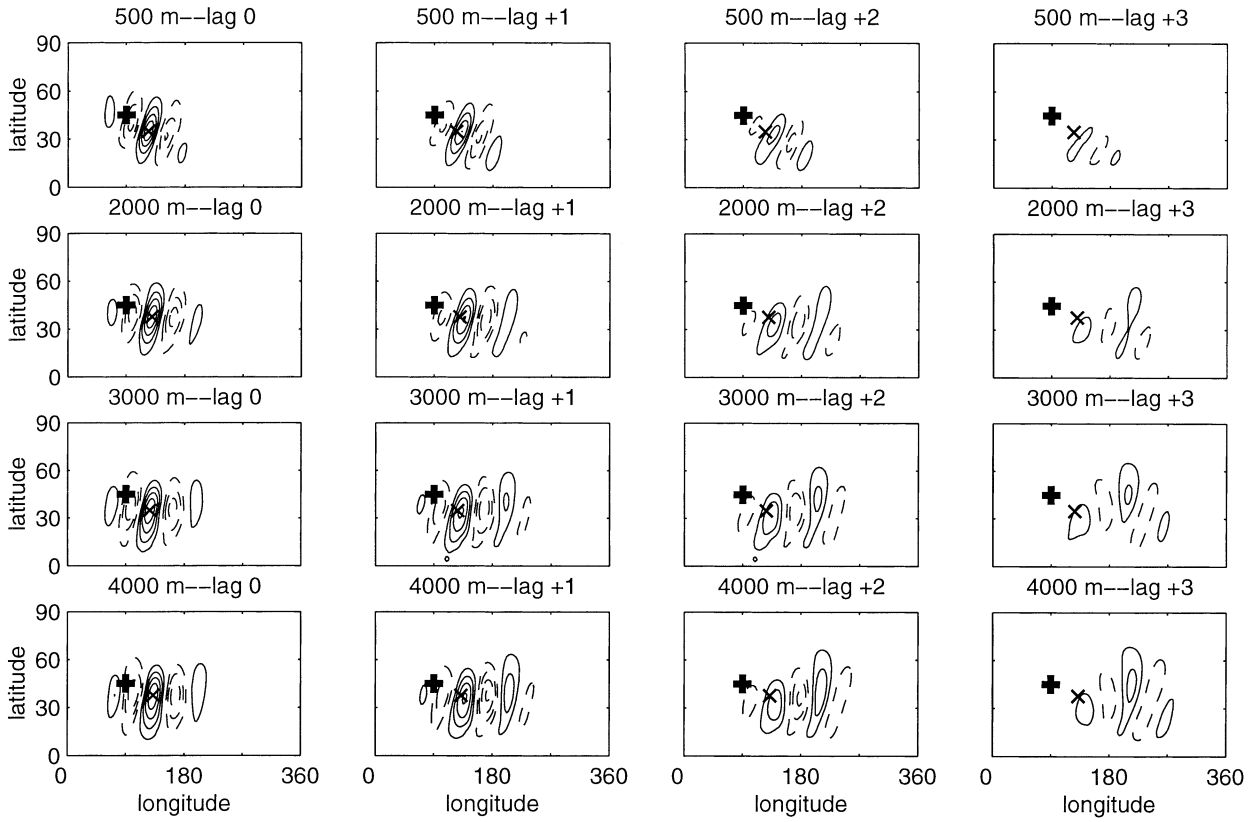

FIG. 5. Eddy meridional wind lag correlations for the (top row) 500-m case, (second row) 2000-m case, (third row) 3000-m case, and (bottom row) 4000-m case. Lags considered are (left-most column) 0 days, (second column) +1 day, (third column) +2 days, and (right-most column) +3 days. The × indicates the basis point. Contour interval is 0.2 (zero contour omitted). Dashed contours are negative.

200°E; and impacting low latitudes a second time near 20°N, 270°E. As in earlier more idealized studies, a comparison of the 2000-, 3000-, and 4000-m cases for a given lag (e.g., +3 days) reveals that the amplitude of the reflected wave increases with the height of the mountain.

The spatial structure of the reflected wave shown in Fig. 5 is very similar to that observed in previous studies. Compare, for example, the wave train in the 4000-m, lag +3 case with the reflected wave in Fig. 10 in Brunet and Haynes (1996), Fig. 15 in Magnusdottir and Haynes (1999), and Fig. 10 in Magnusdottir and Walker (2000). In spite of the different models used in these studies, the signature of the reflected wave is similar in each case. This is to be expected, since the studies all use the same shape topography and consider the wintertime Northern Hemispheric flow. The similarity between our study and the previous studies, however, does lend credence to our claim that nonlinear reflection explains the correlation patterns in Fig. 5.

Note that for all three of the large-amplitude mountains (2000, 3000, and 4000 m), the signal is a superposition of a reflected wave and a wave that penetrates deep into low latitudes and is dissipated near its critical line. This is seen, for example, in the lag +3 case for the 2000-m mountain. In addition to the weak reflected wave train propagating northeast out of the wave breaking region, a second wave is visible propagating southeast deep into the low latitudes. This second wave is apparent in the region of positive correlation centered around 30°N, 200°E. The southern lobe of this region has a southwest to northeast tilt, indicating equatorward propagation.

The superposition is a consequence of variations in the zonal wind near the topography. As mentioned earlier, the amplitude of a topographically excited wave depends on the strength of the zonal wind in the vicinity of the topography. In this case, transient baroclinic disturbances lead to fluctuations in the zonal wind, and therefore to changes in the strength of the resulting wave. Waves of sufficient amplitude break as they approach their critical line, leading to the reflection documented above. On the other hand, provided that there is a gradient of PV at low latitudes, small-amplitude waves penetrate deep into low latitudes, where they are dissipated near their critical line. For the 500-m mountain, the wave amplitude is never large enough to cause wave breaking, and therefore the solution does not have a reflected component, only the wave that propagates deep into the low latitudes. In contrast, both possibilities occur for the 2000-, 3000-, and 4000-m cases, leading to the superposition of the two solutions.

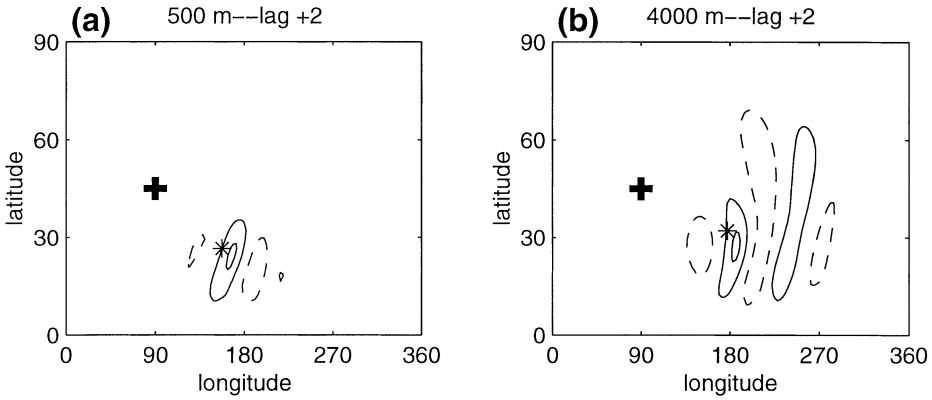

FIG. 6. Eddy meridional wind lag correlations (+2 days) for the (a) 500-m case and (b) 4000-m case. The * indicates the basis point. Contour interval is 0.2 (zero contour omitted). Dashed contours are negative.

To demonstrate that our conclusions are independent of the location of the basis point, we present correlations generated using a second basis point. This basis point is at the center of the southernmost region of negative eddy meridional wind and is shown in Figs. 2a and 3c with an asterisk (*). For brevity, we only show results for the lag +2 correlation of the 500- (Fig. 6a) and 4000-m (Fig. 6b) mountains. These figures show broadly the same patterns as in Fig. 5. In the small-amplitude case (500 m), the topographically excited wave is dissipated near the critical line. The 4000-m case again shows a wave propagating out of the low-latitude wave breaking region into midlatitudes. The superposition mentioned earlier is more visible with this basis point: in this case, the equatorward propagating wave is of roughly the same amplitude as the reflected wave.

4. Concluding remarks

Using an atmospheric GCM with axisymmetric boundary conditions, we have shown that planetary waves are nonlinearly reflected out of the low-latitude wave breaking region. This is in agreement with a suite of earlier studies in more idealized models (Brunet and Haynes 1996; Magnusdottir and Haynes 1999; Magnusdottir and Walker 2000; Walker and Magnusdottir 2002). We have extended these earlier studies by demonstrating that reflection occurs even in the more realistic setting of an atmospheric GCM. Although the GCM has a simplified lower boundary and is run in perpetual January mode, it is otherwise standard, with all of the processes normally associated with a GCM. Specifically, we have shown that nonlinear reflection exists even in the presence of high-frequency transients, which have been shown to have strong interactions with planetary waves (e.g., Branstator 1992).

Our results are in conflict with those of CH92, who examined the nonlinear response of a simplified GCM to idealized topographical forcing and did not find nonlinear reflection. This motivates the following question: Why do we see nonlinear reflection while, in very similar experiments, CH92 do not? CH92 pointed out two factors that may have artificially suppressed nonlinear reflection in their experiments and might therefore explain why the two studies arrive at different conclusions. First, CH92 forced their model with annually averaged solar radiation, leading to a very weak Hadley circulation (upper tropospheric meridional wind speed of less than 0.5 m s^{-1}). Studies with simple mechanistic models have indicated that a weak Hadley circulation is associated with a low-latitude flow that does not conserve angular momentum and, consequently, has a steep low-latitude PV gradient (e.g., Fang and Tung 1999). A steep low-latitude PV gradient is resistant to wave breaking and therefore to wave reflection, which depends on PV overturning. CH92 suggested that a stronger Hadley circulation might give a weaker low-latitude PV gradient, leading to increased PV overturning and nonlinear reflection.

To test CH92's idea that the Hadley circulation sets the low-latitude PV gradient and thus exerts a control on nonlinear reflectivity, we conducted experiments (not shown) where our model was forced with the solar radiation of 15 July. The results of these experiments do not support CH92's hypothesis. Although the Hadley circulation is weak (upper tropospheric meridional wind speed of less than 0.5 m s^{-1}), the low-latitude PV gradient in this case is slightly shallower than that of the corresponding 15 January experiments. Accordingly, we find that nonlinear reflection in these experiments is as robust as the reflection shown in section 3.

Although we found that the strength of the Hadley circulation does not explain the discrepancies between our results and those of CH92, the underlying idea that the discrepancies are due to differences in the low-latitude PV gradient may still be valid. The zonal wind in CH92's time-averaged flow is quite different than the zonal wind shown in Fig. 1a. It may be that the low-latitude PV gradient in their case is steeper than in our

case. Unfortunately, CH92 do not show their PV profile, so that no comparison can be made.

CH92 also suggest that the coarse horizontal resolution (R15) used in their experiments may have played a role in preventing reflection. To test this hypothesis, we duplicated several of the experiments considered in section 3 at T21 spectral resolution (not shown), where the gridpoint resolution of T21 (5.6° × 5.6°) is similar to that of R15 (4.5° × 7.5°). Although the reflected wave is weaker at T21 than in the equivalent T42 case, reflection still takes place.

In addition to the basic state and resolution, there are other factors that may have contributed to the discrepancies between the two studies. The model used by CH92, for example, is considerably older than the model used in this study, and advances in the various parameterization schemes may be significant. In addition, CH92 prescribe zonally symmetric clouds, while the clouds in our model are dynamically determined and are not zonally symmetric. The treatment of surface heat flux is another difference between the two studies. In CH92, the surface has no heat capacity, while in our case, the surface has infinite heat capacity. Although these factors are of secondary importance to the basic state, they may be significant.

Based on our results, we believe that nonlinear planetary wave reflection plays a role in setting the time-averaged wintertime circulation. The wave amplitudes for the 2000-, 3000-, and 4000-m cases are consistent with the observed stationary wave amplitudes. Furthermore, the model basic state, shown in Figs. 1a and 1b, is in accord with the observed zonally averaged Northern Hemisphere wintertime flow. The simplifications made to the model—perpetual January solar radiation and simplified boundary conditions—are made only to isolate and amplify the signal due to reflection. We therefore believe that the model represents the real wintertime atmosphere and that nonlinear reflection is likely occurring in the real atmosphere.

Acknowledgments. This work was supported by NSF Grant ATM-9908883 and by NASA Grant NGT5-03203. An allocation of computer time was made by the Scientific Computing Division of the National Center for Atmospheric Research. We thank Dr. Jeff Yin for advice on setting up the model. We thank Dr. Ed Schneider and an anonymous reviewer for helpful comments on the manuscript.

REFERENCES

Blackmon, M. L., Y.-H. Lee, J. M. Wallace, and H.-H. Hsu, 1984: Time variation of 500 mb height fluctuations with long, intermediate and short time scales as deduced from lag-correlation statistics. *J. Atmos. Sci.,* **41,** 981–991.

Branstator, G., 1992: The maintenance of low-frequency, atmospheric anomalies. *J. Atmos. Sci.,* **49,** 1924–1945.

Brunet, G., and P. H. Haynes, 1996: Low-latitude reflection of Rossby wave trains. *J. Atmos. Sci.,* **53,** 482–496.

Charney, J. G., and A. Eliassen, 1949: A numerical method for predicting the perturbations of the middle latitude westerlies. *Tellus,* **1,** 38–54.

Cook, K. H., and I. H. Held, 1992: The stationary response to large-scale orography in a general circulation model and a linear model. *J. Atmos. Sci.,* **49,** 525–539.

Esler, J. G., L. M. Polvani, and R. A. Plumb, 2000: The effect of the Hadley circulation on the propagation and reflection of planetary waves in a simple one-layer model. *J. Atmos. Sci.,* **57,** 1536–1556.

Fang, M., and K. K. Tung, 1999: Time-dependent nonlinear Hadley circulation. *J. Atmos. Sci.,* **56,** 1797–1807.

Grose, W. L., and B. J. Hoskins, 1979: On the influence of orography on the large-scale atmospheric flow. *J. Atmos. Sci.,* **36,** 223–234.

Held, I. M., 1983: Stationary and quasi-stationary eddies in the extratropical atmosphere: Theory. *Large-Scale Dynamical Processes in the Atmosphere,* B. Hoskins and R. Pearce, Eds., Academic Press, 127–168.

——, and P. J. Phillips, 1990: A barotropic model of the interaction between the Hadley cell and a Rossby wave. *J. Atmos. Sci.,* **47,** 856–869.

Killworth, P. D., and M. E. McIntyre, 1985: Do Rossby-wave critical layers absorb, reflect, or over-reflect? *J. Fluid Mech.,* **161,** 449–492.

Magnusdottir, G., and P. H. Haynes, 1999: Reflection of planetary waves in three-dimensional tropospheric flows. *J. Atmos. Sci.,* **56,** 652–670.

——, and C. Walker, 2000: On the effects of the Hadley circulation and westerly equatorial flow on planetary-wave reflection. *Quart. J. Roy. Meteor. Soc.,* **126,** 2725–2745.

Postel, G. A., and M. H. Hitchman, 1999: A climatology of Rossby wave breaking along the subtropical tropopause. *J. Atmos. Sci.,* **56,** 359–373.

Randel, W. J., 1987: A study of planetary waves in the southern winter troposphere and stratosphere. Part I: Wave structure and vertical propagation. *J. Atmos. Sci.,* **44,** 917–935.

Schneider, E. K., 1990: Linear diagnosis of stationary waves in a general circulation model. *J. Atmos. Sci.,* **47,** 2925–2952.

Shea, D. J., K. E. Trenberth, and R. W. Reynolds, 1990: A global monthly sea surface temperature climatology. NCAR Tech. Note 345+STR, 167 pp.

Smagorinsky, J., 1953: The dynamical influence of large-scale heat sources and sinks on the quasi-stationary mean motions of the atmosphere. *Quart. J. Roy. Meteor. Soc.,* **79,** 342–366.

Walker, C. C., and G. Magnusdottir, 2002: Effect of the Hadley circulation on the reflection of planetary waves in three-dimensional tropospheric flows. *J. Atmos. Sci.,* **59,** 2846–2859.

Waugh, D. W., and L. M. Polvani, 2000: Climatology of intrusions into the tropical upper troposphere. *Geophys. Res. Lett.,* **27,** 3857–3860.

Yin, J. H., and D. S. Battisti, 2001: A detailed GCM study of the factors influencing the location and strength of the storm tracks. Preprints, *13th Conf. on Atmospheric and Oceanic Fluid Dynamics,* Breckenridge, CO, Amer. Meteor. Soc., 279–282.